Effect of Discontinuous Edge Obstacles on Flow Patterns and Energy Dissipation in Stepped Spillways

Seyed Amin Asghari Pari[1*], Mojtaba Kordnaeij[2] and Ram Balachandar[3]

1- Corresponding author, Associate Professor, Department of Civil Engineering, Faculty of Engineering, Behbahan Khatam Alanbia University of Technology, Behbahan, Iran. (asghari_amin@bkatu.ac.ir).*

2- Lecturer, Department of Civil Engineering, Faculty of Engineering, Behbahan Khatam Alanbia University of Technology, Behbahan, Iran.

3- Distinguished University Professor, Department of Civil and Environmental Engineering, University of Windsor, Windsor, Ontario, Canada.

ARTICLE INFO

Article history:
Received:
Revised:
Accepted:
Available online:

Keywords:
stepped spillway; energy dissipation; discontinuous obstacle; transverse flow; bubble image velocimetry

TO CITE THIS ARTICLE:

Abstract

The hydraulic effects of discontinuous edge obstacles on stepped spillways were quantified experimentally. A total of 384 tests were conducted in a 1.2 m-wide flume for two chute geometries: 1V:2H (θ = 27.5°) and 1V:3H (θ = 19.2°). Obstacle length l_o, obstacle height h_o, flume width w, and step height h were varied over l_o/w = 0.05–0.50 and h_o/h = 0.19–0.74. Bubble Image Velocimetry (BIV) measurements between Steps 6 and 7 showed that transverse redirected-flow and mixing zones were generated by discontinuous obstacles; consequently, multi-wavy and staggered three-dimensional flow patterns that were absent for flat steps and continuous obstacles were produced. The best performance within the tested range was obtained at l_o/w = 0.25 and h_o/h = 0.56. At d_c/h = 1.06, relative energy dissipation on the 1V:3H spillway was increased from 46.09% for flat steps to 65.20% for the optimal discontinuous configuration, corresponding to a gain of 19.11 percentage points (41.5% relative). On the 1V:2H spillway, an increase from 39.74% to 49.15% was obtained, corresponding to a gain of 9.41 percentage points (23.7% relative). The systematic two-slope comparison and the BIV-based visualization therefore demonstrated that discontinuous obstacles were particularly effective on the milder 1V:3H spillway.

Article Highlights

- A systematic two-slope dataset was developed from 384 tests covering l_o/w = 0.05–0.50 and h_o/h = 0.19–0.74.
- Transverse RFT and MZT regions, multi-wavy flow, and staggered three-dimensional surface patterns were generated by discontinuous obstacles.
- At d_c/h = 1.06, gains of 19.11 and 9.41 percentage points were produced by the optimal configuration on the 1V:3H and 1V:2H spillways, respectively.

Introduction

Flow energy is dissipated by stepped spillways through step-induced macro-roughness, air entrainment, and intense momentum exchange. Compared with smooth chutes, the residual kinetic energy is reduced by these mechanisms, and the required size of the downstream stilling basin may be decreased (Chanson, 2001; Boes & Hager, 2003a; Chanson, 2006; Meireles & Matos, 2009; Frizell et al., 2013; Felder & Chanson, 2016). In skimming flow, the main stream is conveyed over a pseudo-bottom while recirculating flow is retained within the step cavities (Chanson, 2002). The principal geometric and flow features used in this study

are defined in Figure (1), including the step height h, step length L, number of steps N, recirculation zone, mixing zone, pseudo-bottom, and inception point of free-surface aeration.

Flow regimes, momentum exchange, aeration inception, cavitation, and energy dissipation have been addressed in research on stepped spillways. Modification of air-water flow over stepped chutes by macro-roughness and staggered arrangements was shown by Kökpinar (2004) and Andre et al. (2004). Velocity and pressure fields in skimming flow were characterized by Amador et al. (2004a), and changes in skimming-flow structure caused by step roughness were demonstrated by Gonzalez et al. (2005), while the promotion of three-dimensional turbulence by staggered baffles was reported by Gonzalez and Chanson (2007). Energy dissipation upstream of the inception point on flat-sloped stepped spillways was quantified by Hunt and Kadavy (2010), and a shorter distance to aeration inception and reduced downstream scour were reported by Wright (2010) for triangular protrusions. Pooled steps, baffle blocks, end sills, and staggered macro-roughness were subsequently examined by Felder et al. (2012), Zare and Doering (2012), and Guenther et al. (2013); enhanced aeration and turbulence were reported, although the energy-dissipation benefit was found to depend strongly on geometry and flow regime. Prototype-scale air entrainment was subsequently discussed by Chanson (2022).

The range of roughness concepts was extended in later studies. Inclined steps with end sills were evaluated by Hamedi et al. (2014), porous pooled configurations were studied by Felder and Chanson (2014, 2015), and pooled steps and breakers were investigated by Krisnayanti et al. (2016) and Abdel Aal et al. (2018). Pooled-step geometry was numerically linked to turbulence and air–water flow by Li and Zhang (2018) and Li et al. (2018). Gabion-step free-surface, cavity, and seepage interactions were examined by Zhang and Chanson (2016). A 1.2 m-wide flume was used by Asghari Pari and Kordnaeij (2021), and the creation of wavy and transverse flow by discontinuous obstacles, as well as their potential to outperform continuous obstacles, was demonstrated; however, the tested dimensional range was limited. An increase in dissipation caused by step-mounted roughness, particularly in skimming flow, was further demonstrated by Kordnaeij et al. (2023). A chronological summary of the main obstacle-related studies is provided in Table (1), in which the principal test variables and measurement methods are reported.

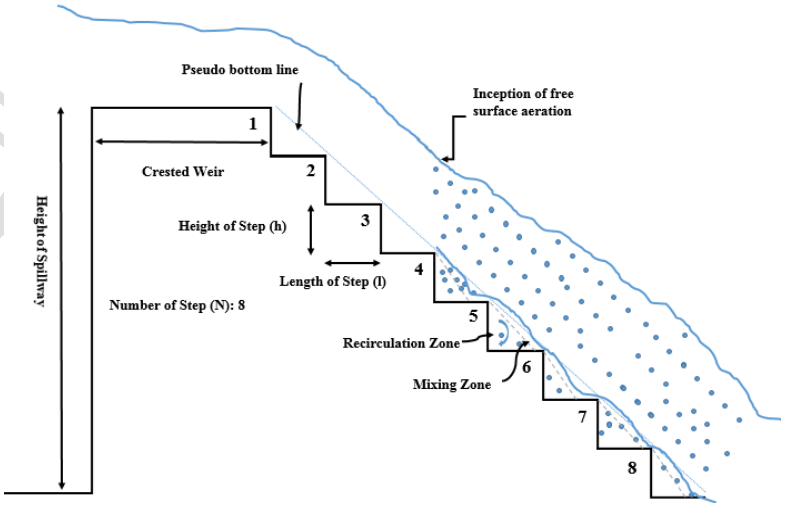


Fig. 1- Schematic of flow components on a flat-step spillway.

Table 1- Summary of experimental studies on the effects of obstacles located on the edges of stepped spillways.

Reference	θ (°)	W (m)	H (m)	q (m²/s)	d_c/h (-)	h_o/h (-)	Instrument	Configuration
Kökpinar (2004)	30	0.5	3.84	0.06 to 0.2	----	0.5	Double-tip fiber-optical probe	Pooled without strip macro-roughness
Andre et al. (2004)	30	0.5	4	0.02 to 0.28	-----	0.43 and 0.5	Double-tip fiber-optical probe	Pooled–staggered with macro-roughness
Felder et al. (2012)	8.9	0.5	1	0.054 to 0.234	1 to 3.35	1	Double-tip fiber-optical probe	Combination of flat and pooled steps
Zare and Doering (2012)	45	0.57	0.823	0.012 to 0.225	0.4 to 2.5	0.25	Point gauge and ultrasonic depth meter	Baffle blocks and end sill
Guenther et al. (2013)	26.6	0.52	0.9	0.01 to 0.219	1.1 to 1.5	0.31	Double-tip fiber-optical probe	Pooled–staggered
Hamedi et al. (2014)	18.4	1.33	2.796	0.023 and 0.068	----	0.13-0.17-0.21-0.32	Liminimeter, a pitot-tube and point gage	Inclined steps with end sill
Felder and Chanson (2014)	8.9 26.6	0.5 1	1 0.9	0.1 to 0.18		0.31	Double-tip fiber-optical probe	Pooled–porous
Felder and Chanson (2015)	3.4 to 26.6	0.5,0.52 and 1	0.87, 0.9 and 1	0.003 to 0.282	0.13 to 3.54	0.31	Double-tip fiber-optical probe	Pooled–porous
Krisnayanti et al. (2016)	45	0.5	2	0.007 to 0.061	0.7 to 3	0.15	Point gauge	Pooled
Abdel Aal et al. (2018)	29.05	0.65	0.3	0.02 to 0.09		0.2 - 0.4 - 0.6 0.8 and 1	Point gauge	Pooled–porous breakers
Li and Zhang (2018)	26.6	0.52	0.9	0.219	1.5	0.9	Numerical	Pooled steps and weir
Asghari Pari and Kordnaeij (2021)	19.2, 27.5	1.2	0.87-0.88	0.035 to 0.122	0.46 to 1.06	0.19 - 0.74	Point gauge and BIV	Porous screen, continuous obstacle, and continuous porous obstacle
Sánchez-Juny et al. (2022)	51.3	1.0 to 3.0	5.0	0.085 to 0.26	1.13 to 2.38	-	BIV	Pooled steps without sidewall constraint
Kordnaeij et al. (2023)	19.2, 27.5	1.2	0.87 to 0.88	0.035 to 0.122	0.46 to 1.06	0.2 to 0.7	Point gauge and BIV	Step-mounted roughness
Mikalsen et al. (2024)	51	1.0	1.2	0.057 to 0.485	0.8 to 3.3	----	BIV & ADV	Crest splitters
Current study	19.2 27.5	1.2	0.87-0.88	0.035 to 0.122	0.46 to 1.06	0.19 - 0.38-0.56 and 0.74	Point gauge and BIV	Discontinuous obstacles

Notes: θ = spillway inclination angle; w = flume width; H = spillway height; q = discharge per unit width; d_c = critical depth; h = step height; h_o = obstacle height.

Velocity measurements in stepped-spillway flows have been improved by non-intrusive image-based techniques, but their applicability is governed by the local air concentration. Particle Image Velocimetry (PIV) is considered appropriate in non-aerated or weakly aerated regions, whereas conventional tracer detection in strongly aerated flow is limited by bubble interference (Chang & Liu, 1998; Amador et al., 2004b). PIV was applied by Habibi et al. (2025) to non-aerated skimming-flow regions of a stepped spillway, and this application domain was thereby illustrated. In Bubble Image Velocimetry (BIV), introduced by Ryu et al. (2005), entrained air bubbles are instead used as tracers; therefore, aerated regions can be investigated. BIV was applied by Asghari Pari and Kordnaeij (2021) in a 1.2 m-wide flume to characterize the wavy and transverse

aerated flow generated by discontinuous obstacles. BIV has also been used in stepped-spillway studies by Leandro et al. (2014), Bühler et al. (2015), Bung and Valero (2015, 2016a), Lopes et al. (2015, 2017), Sánchez-Juny et al. (2022), Mikalsen and Thorsen (2023), and Mikalsen et al. (2024); optical-flow processing of aerated spillway images was reported by Bung and Valero (2016b) and Zhang and Chanson (2018). Thus, the PIV and BIV studies cited here are regarded as methodologically complementary: non-aerated flow is addressed by the former, whereas aerated flow is addressed by the latter. A summary of the relevant image-processing studies is provided in Table (2).

Despite these advances, systematic data remain limited for discontinuous edge-mounted obstacles over a broad range of relative lengths and heights and for direct comparisons between spillway slopes. This gap is addressed in the present study through 384 experiments covering l_o/w = 0.05–0.50, h_o/h = 0.19–0.74, and two slopes (1V:2H and 1V:3H) in a 1.2 m-wide flume. The following objectives were pursued: the effects of obstacle dimensions on aeration inception, flow-regime boundaries, and energy dissipation were quantified; the induced three-dimensional flow structures were characterized using BIV; and the manner in which spillway slope modifies obstacle effectiveness was determined. Novelty is provided by the combined systematic parametric mapping, direct two-slope comparison, and BIV-based linkage between transverse flow structures and measured energy dissipation.

Materials and Methods

The experiments were conducted in a large-scale flume measuring 10 m in length, 1.2 m in width, and 1.0 m in depth. The sidewall height was increased to 1.2 m along the first 3 m of the flume. Discharge was measured using a TFM3100 ultrasonic flowmeter (ADAK Tajhiz Iranian, Iran), with an accuracy of ±1% of the reading and a repeatability of ±0.2%. The maximum flow rate supplied to the flume was 180 *L*/s. The flume sidewalls were constructed of 10-mm-thick transparent glass. To minimize light reflection and enhance image contrast, the back wall in the spillway section was painted matte black. Water depths were measured using a point gauge with an accuracy of ±1 mm. Flow straighteners and turbulence manipulators were installed in the upstream section of the flume, and the spillway was positioned 1.5 m downstream of the start of the rectangular cross-section. The total spillway height *H*, step height *h*, horizontal step length *L*, number of steps *N*, and inclination angle θ are summarized in Table (3).

Table 2- Summary of experimental studies of air-water flow properties on stepped spillways using various image-processing techniques (BIV, IPP, OF, and VC).

Reference	θ (°)	w (m)	q (m²/s)	d_c/h (-)	Method
Leandro et al. (2014)	18.4; 26.6	0.3	0.07 to 0.11	1.3 to 3.6	BIV
Bung and Valero (2015)	26.6	0.5	0.07	1.3	BIV
Lopes et al. (2015)	18.4; 26.6	0.3; 0.5	0.07	1.3	BIV
Bühler et al. (2015)	26.6	0.3	0.09	1.3	IPP
Bung and Valero (2016a)	26.6	0.3; 0.5	0.07	1.3	BIV/OF
Bung and Valero (2016b)	26.6	0.5	0.07	1.3	OF
Lopes et al. (2017)	26.6	0.5	0.07	1.3	BIV
Kramer and Chanson (2018a)	45.0	0.985	0.067	0.8	OF
Kramer and Chanson (2018b)	48	0.99	0.067	0.8	VC
Zhang and Chanson (2018)	45.0	0.985	0.083	0.9	OF
Asghari Pari and Kordnaeij (2021)	19.2; 27.5	1.2	0.035-0.122	0.46-1.06	BIV
Sánchez-Juny et al. (2022)	51.3	1.0 to 3.0	0.085 to 0.26	1.13 to 2.38	BIV
Kordnaeij et al. (2023)	26.6	1.2	0.04–0.09	0.8–1.5	BIV
Mikalsen et al. (2024)	51	1.0	0.057 to 0.485	0.8 to 3.3	BIV
Habibi et al. (2025)	26.6	1.2	0.03–0.08	0.5–1.2	PIV
Current Study	19.2; 27.5	1.2	0.035–0.122	0.46 to 1.06	BIV

Notes: BIV = Bubble Image Velocimetry; IPP = Image Processing Procedure; OF = Optical Flow; PIV = Particle Image Velocimetry; VC = video correlation

Table 3- Spillway Geometry

Slope	θ (°)	H (m)	h (cm)	L (cm)	N
1V:2H	27.5	0.87	10.9	20.9	8
1V:3H	19.2	0.88	10.9	31.3	8

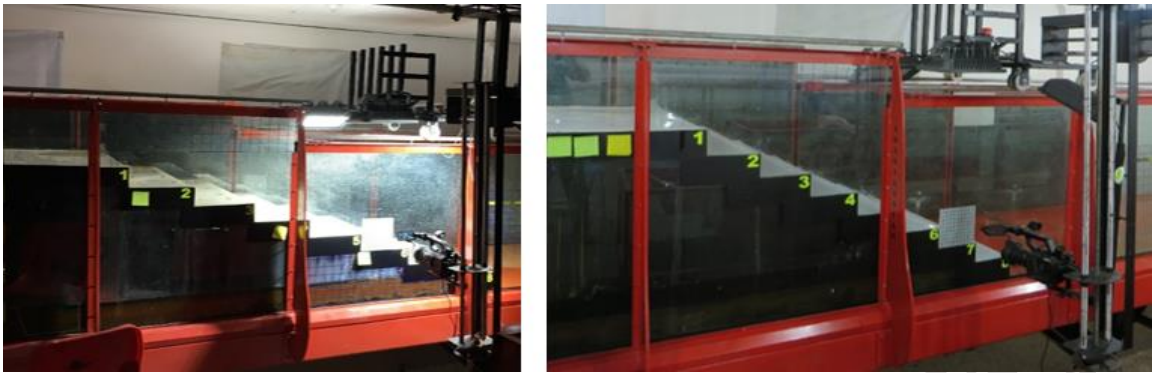


Fig. 2- Flume, spillway, LED, rail and location of camera. Left: θ =19.2° (1:3), Right: θ =27.5° (1:2)

The spillway installed in the flume is shown in Fig. (2). The length of the broad-crested weir located upstream of both spillways was 580 mm to control the discharge (Felder, 2013), and the critical depth over the weir was measured as recommended by Felder (2013). As shown in Fig. (2), the steps were numbered starting from the edge of the broad-crested weir.

A Sony FS5 camera (maximum 965 frames per second) equipped with an AT-X11-20mm PRO DX lens (Tokina) was used for imaging. For illuminating the imaging area, three LED150 projectors were utilized. The first projector was positioned directly above, perpendicular to the imaging plane. The second projector was placed above and inclined at approximately 30° to the horizontal, and the third was positioned outside the flume behind the camera at 60° to the longitudinal axis of the flume. These angles were determined after several trials to achieve optimal lighting conditions for tracing air bubbles while avoiding reflection issues from the glass sidewall.

The camera was mounted on a traversing rail. The transverse distance between the flume sidewall and the camera was set to 0.5 m, as suggested by Bung and Valero (2015) and Emadzadeh and Chiew (2017). Imaging was performed between steps 6 and 7, where fully developed flow and a stable recirculation zone containing air bubbles were observed. The imaging location was 3 mm from the flume wall (Bung & Valero, 2015; Kramer & Chanson, 2018b). A 200 mm × 200 mm grid sheet and a 20 mm × 20 mm lattice were used for image focusing and scaling. In each experiment, the camera focus and alignment were carefully calibrated prior to initiating the flow.

BIV measurements in this study were focused on steps 6 and 7 (out of 8 total steps) because air entrainment was consistently observed at these steps under all tested conditions, rendering them suitable for the analysis of aerated flow and energy dissipation.

The flow-rate range in this study was selected so that all three flow regimes—nappe flow, transitional flow, and skimming flow (Ohtsu & Yasuda, 1997; Chanson, 2002)—were represented.Owing to facility constraints, testing was limited to the lower and intermediate skimming regimes ($dc/h \leq 1.06$); obstacle effectiveness could be altered by higher discharges, for which further investigation is warranted. Experiments were first performed for the flat-step configuration, after which obstacles with different heights were examined. Different heights were produced by stacking pieces of wood with a cross-section of 20 × 20 mm². The range of dc/h was 0.46–1.06. The critical depth formed at the spillway entrance is denoted by dc. The relative obstacle height (obstacle height to step height, h_o/h) was varied from 0.19 to 0.74, and the relative obstacle length (obstacle length to flume width, l_o/w) was varied from 0.05 to 0.50.

Additional experiments were conducted with a continuous obstacle. In total, 384 experiments were conducted: 312 with discontinuous obstacles and 72 with continuous-obstacle and flat-step configurations (see Fig. 3).

Results and Discussion

The results are presented in a structured manner, starting with the inception point (IP) of aeration, followed by flow regime determination, internal flow structures from BIV analysis, surface flow patterns, and energy dissipation. Key findings are linked across subsections to highlight the effects of discontinuous obstacles on flow characteristics and performance.

Inception Point of Free-Surface Aeration (IP)

The inception of aeration was determined visually. At d_c/h = 1.06, the inception point (IP) was recorded one step farther downstream on the 1V:2H spillway than on the 1V:3H spillway under flat-step conditions (Appendix Table A1). When a continuous obstacle (l_o/w = 1) was placed on the spillway edge, the IP was shifted one additional step downstream on both slopes. Discontinuous obstacles generally produced little change in the IP on the 1V:3H spillway; however, selected increases in obstacle height shifted the IP one step upstream on the 1V:2H spillway. An upstream shift in the IP may reduce cavitation exposure on the initial non-aerated steps and may enhance energy dissipation through earlier air entrainment. A visual comparison of the inception point for different discontinuous-obstacle configurations under a constant-flow condition is provided in Figure (4).

Non-uniform aeration across the step width was observed with discontinuous obstacles. At the steps where aeration was initiated, air was entrained only downstream of locations at which an obstacle had been placed upstream, whereas no aeration was observed in the unobstructed areas. This asymmetry at Step 2 for the 1:3 slope, dc/h = 1.06, h_o/h = 0.74, and l_o/w = 0.5 is illustrated in Figure (5).

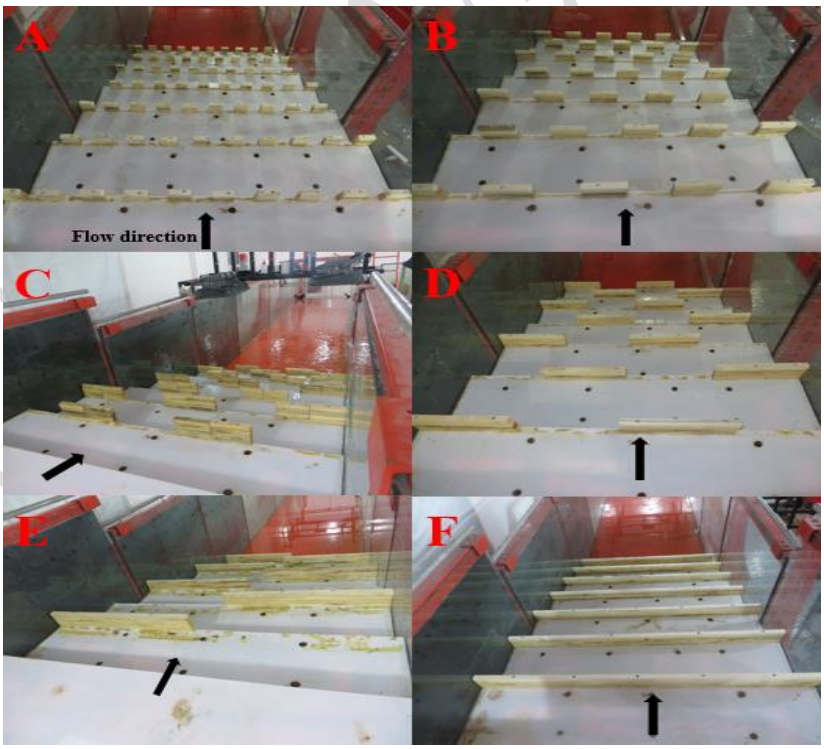


Fig. 3- Model configurations for the 1V:3H slope: A, l_o/w = 0.05; B, 0.10; C, 0.20; D, 0.25; E, 0.50; F, 1.00.

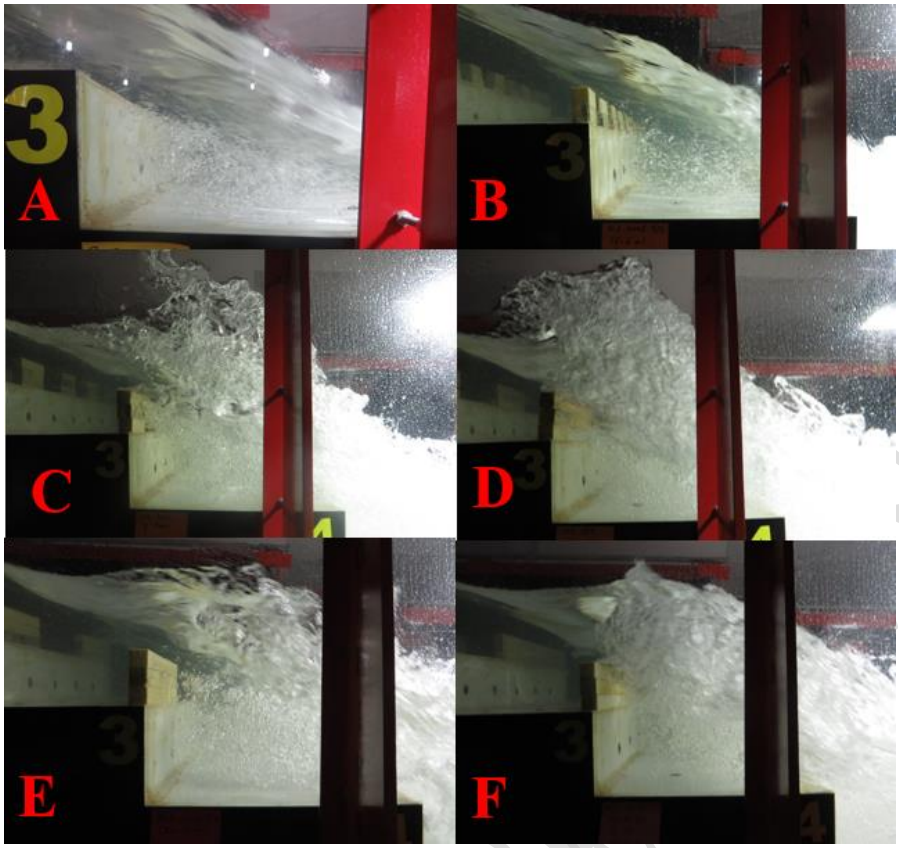


Fig. 4- Inception point for discontinuous-obstacle configurations on the 1V:3H spillway at dc/h = 1.06 and h_o/h = 0.56: A, flat step; B, l_o/w = 0.05; C, 0.10; D, 0.20; E, 0.25; F, 0.50.

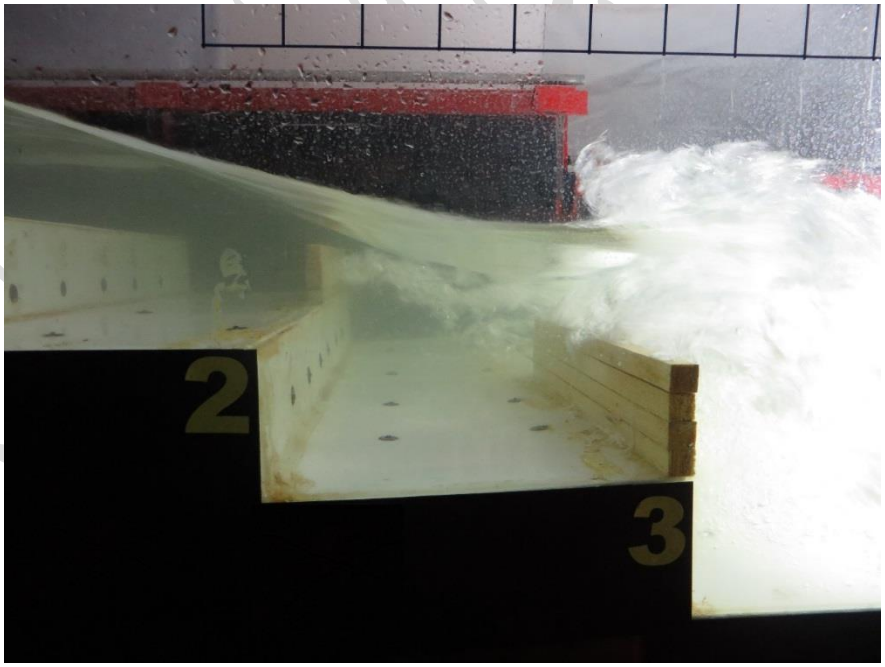


Fig. 5- Asymmetry of the inception point on the 1V:3H spillway at dc/h = 1.06, h_o/h = 0.74, and l_o/w = 0.50.

The inception-point observations are summarized in Appendix Table (A1).

Flow Regime Determination

Criteria for flow regimes have been defined by numerous laboratory experiments on the basis of relative critical depth d_c/h and chute geometry h/L, although variability in the boundaries of transitional and skimming flows has often been introduced by visual observations (Ostad Mirza, 2016). Existing equations proposed by Chanson (1995, 2002) and Ohtsu and Yasuda (1997) were developed primarily for flat-step spillways. In the present study, the manner in which these regimes are altered by obstacles was examined, consistent with previous works (Andre et al., 2004; Zare & Doering, 2012; Kökpinar, 2004). Regimes were classified on the basis of experiments and videos as nappe flow (no aeration), transitional flow (aeration in recirculation zones with air pockets), and skimming flow (no air pockets and recirculation below the pseudo-bottom). The categorizations are presented in Figures (6) and (7).

At the 1V:2H slope (Fig. 6), transitional and skimming regimes were initiated at lower *dc/h* by continuous obstacles than by the flat-step configuration, whereas the flat-step transitional-regime boundary was matched by discontinuous obstacles and the onset of skimming was delayed to higher *dc/h*. For the 1V:3H slope (Fig. 7), regimes were initiated at lower *dc/h* by continuous obstacles at h_0/h = 0.19; with increasing height, the boundaries were shifted to higher *dc/h* and approached the flat-step boundaries. Except at l_0/w = 0.05 and h_0/h = 0.56, the flat-step transitional-onset boundary was matched by discontinuous obstacles, whereas skimming was delayed to *dc/h* values equal to or higher than those of the flat-step configuration. At l_0/w = 0.05, boundaries similar to those of continuous obstacles were obtained because of the close spacing. At the 1V:2H slope, skimming boundaries were shifted to higher *dc/h* by discontinuous obstacles more substantially than at the 1V:3H slope. Similar ranges for l_0/w = 0.5 and h_0/h = 0.31 at a 1:2 slope were reported by Guenther et al. (2013) (nappe: *dc/h* < 0.5; skimming: *dc/h* > 0.92), in agreement with the present results. Existing formulae were found to be ineffective for predicting flow regimes in the presence of continuous or discontinuous obstacles on both slopes. Flow tends to be converted to skimming at lower discharges by continuous obstacles, whereas the transitional-flow range is extended and the flow rate required for skimming is increased by discontinuous obstacles relative to the flat-step configuration.

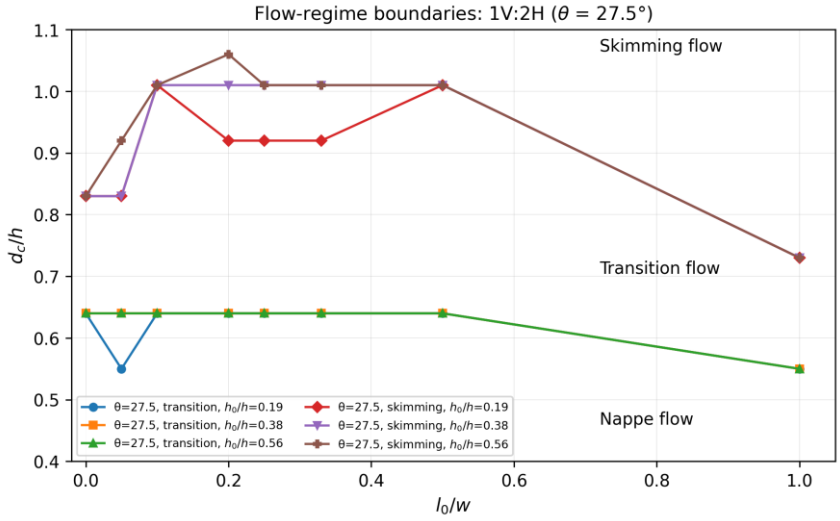


Fig. 6- Onset of the transition and skimming-flow regimes for the 1V:2H spillway (θ = 27.5°).

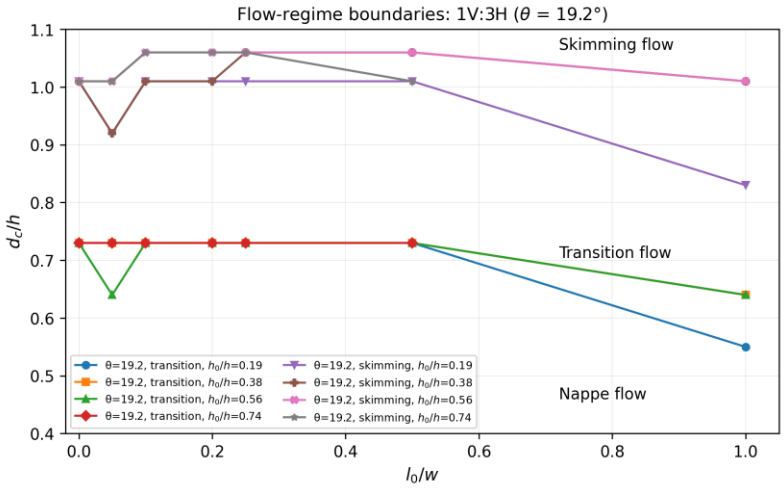


Fig. 7- Onset of the transition and skimming-flow regimes for the 1V:3H spillway (θ = 19.2°).

According to Figures (6) and (7), the onset of the skimming boundary on the 1V:2H slope is shifted to substantially higher *dc/h* by the creation of a discontinuous obstacle, relative to the flat-step configuration and to similar conditions on the 1V:3H slope. These findings are consistent with Guenther et al. (2013), by whom a nappe-flow regime at *dc/h* < 0.5 and a skimming-flow regime at *dc/h* > 0.92 were reported under similar conditions (l_o/w = 0.5, h_o/h = 0.31, 1V:2H slope).

The previously proposed formulae (Chanson, 1995, 2002; Ohtsu & Yasuda, 1997; Andre et al., 2004; Chanson et al., 2015) were shown by the flow-regime analysis to be ineffective for determining the range of flow regimes when continuous or discontinuous obstacles are placed on the spillway edge for either slope. The transition to the skimming regime at lower flow rates (lower dc/h than for the flat-step configuration) is induced by the placement of a continuous obstacle on the spillway edge. In contrast, the transitional-flow range is extended and the flow rate required for skimming is increased by the placement of discontinuous obstacles at the same slopes relative to the flat-step configuration.

Internal Flow Structures and Streamlines via BIV

Mean streamlines were plotted from BIV velocity data to visualize flow conditions under the pseudo-bottom (Figs. 8–13). For the flat-step configuration in skimming flow, two main zones are formed: a recirculation zone (RZ), within which recirculation occurs, and a mixing zone (MZ), within which the flow is impinged on the step floor. RZ and MZ were identified under the pseudo-bottom from the BIV results, and differences in their shape and size between consecutive steps were observed, consistent with the findings of Lopes et al. (2017) for widths of 0.3 m and 0.5 m. In the 1.2 m-wide flume used in the present study, this difference was evident at both slopes, and a longer MZ was observed at 1:3 than at 1:2 (Fig. 8).

The topology of the MZ and RZ was significantly altered by the introduction of obstacles; in some cases, these zones were eliminated entirely and new zones were created. For continuous obstacles, the flow is redirected toward the main stream through interaction with the obstacle, and a redirected-flow (RF) zone is formed. For discontinuous obstacles, in addition to RF, part of the flow is directed toward the unobstructed sides of the steps, and transverse flows are formed across the flume width (Fig. 9A, C). The MZ and RF are modified by these transverse flows, and MZ_T and RF_T zones are created. In some cases, RF and RZ were merged into RZ-RF (Figs. 10C, 11B). Overall, a fully three-dimensional flow field is produced through the interaction of the main flow, RZ, RF_T, and MZ_T (Fig. 9). Differences in flow lines between the 1:3 and 1:2 slopes for similar relative lengths and heights were caused by the longer steps on the 1:3 slope. With increasing continuous-obstacle height, RF was expanded while RZ and MZ were contracted; with further increases, pooled steps with a prominent RZ

were formed (RZ_P; Figs. 10D, 11C, D). RZ_P was formed at h_0/h = 0.74 for 1:3 but at h_0/h = 0.38 for 1:2, indicating a lower height threshold for pooling on the steeper slope. This difference can be attributed to the wider extent covered by RZ in the flat-step configuration at 1:2 than at 1:3 (Fig. 8), through which pooling is allowed at lower obstacle heights.

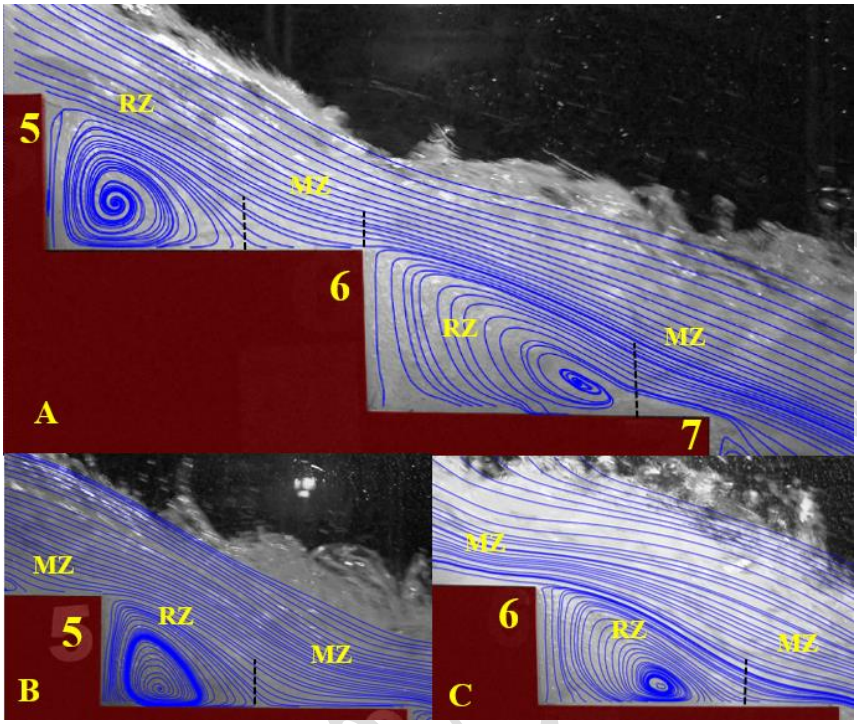


Fig. 8- Comparison of recirculation (RZ) and mixing (MZ) zones on consecutive steps at dc/h = 1.06: A, 1V:2H slope, Steps 6 and 7; B, 1V:3H slope, Step 6; C, 1V:3H slope, Step 7.

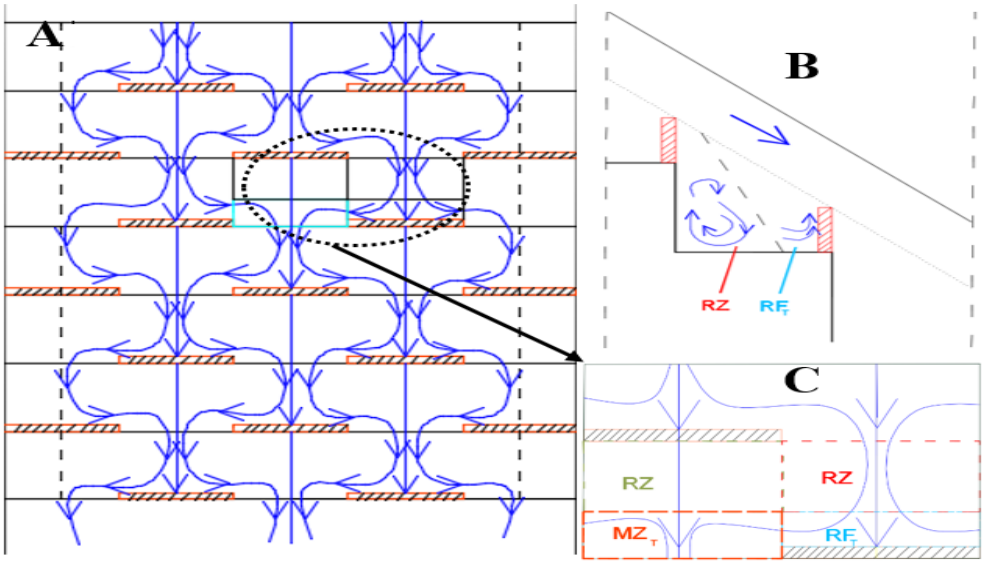


Fig. 9- Schematic of the internal flow structure generated by a discontinuous obstacle (l_0/w = 0.25): A, top view; B, side view; C, detail of the selected region.

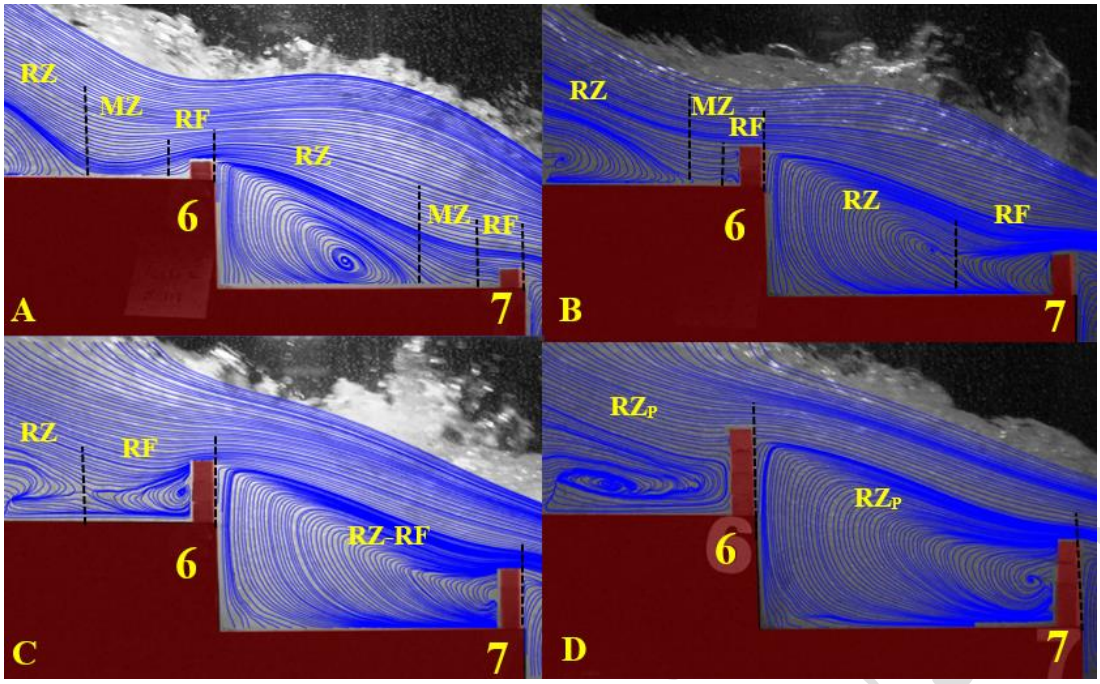


Fig. 10- Comparison of flow zones on Steps 6 and 7 at dc/h = 1.06, 1V:3H slope, and l_o/w = 1: A, h_o/h = 0.19; B, 0.38; C, 0.56; D, 0.74.

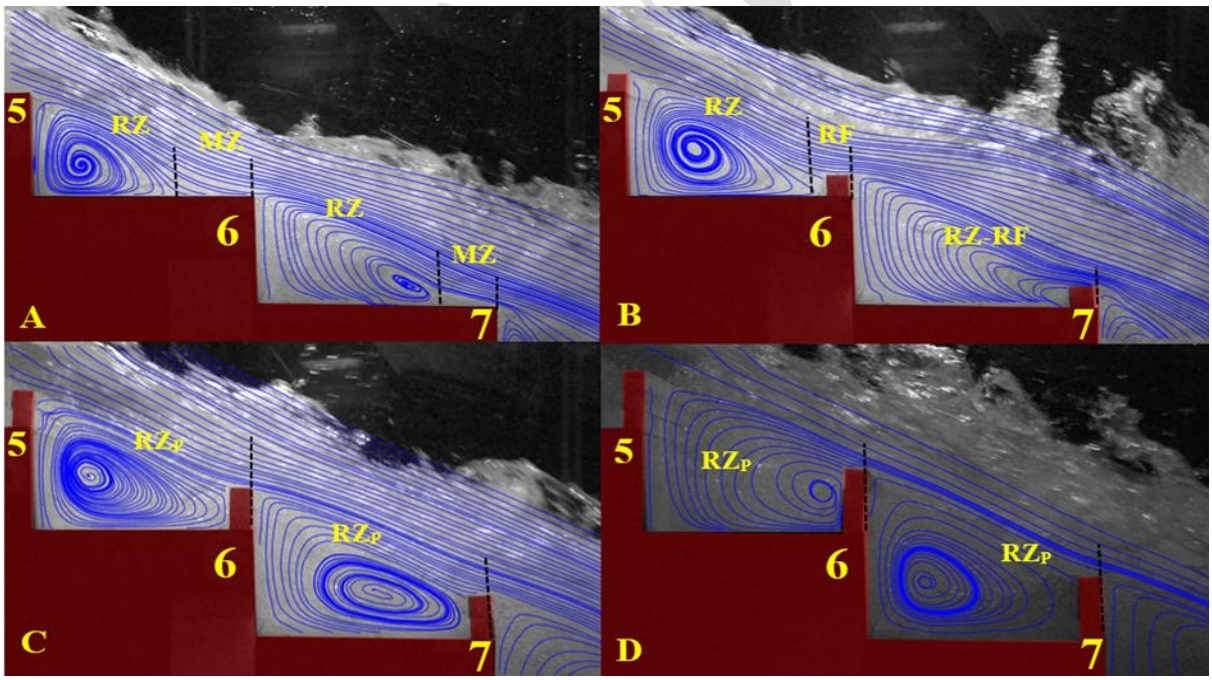


Fig. 11- Comparison of flow zones on Steps 6 and 7 at dc/h = 1.06, 1V:2H slope, and l_o/w = 1: A, flat step; B, h_o/h = 0.19; C, 0.38; D, 0.56.

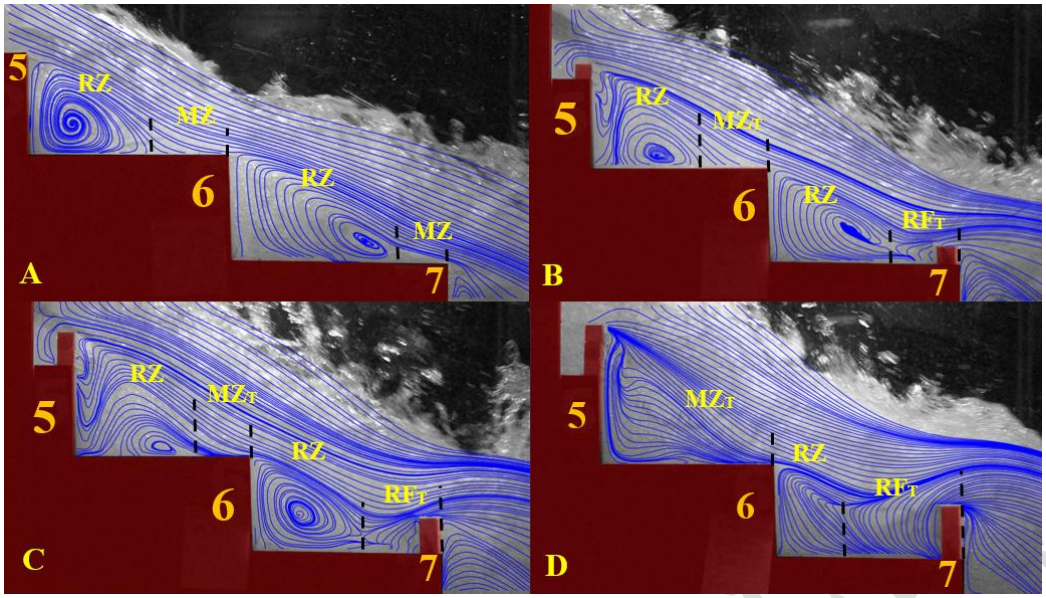


Fig. 12- Comparison of formed flow zones on Steps 6 and 7 at dc/h = 1.06, 1V:2H slope, and l_o/w = 0.25: A, flat step; B, h_o/h = 0.19; C, h_o/h = 0.38; D, h_o/h = 0.56.

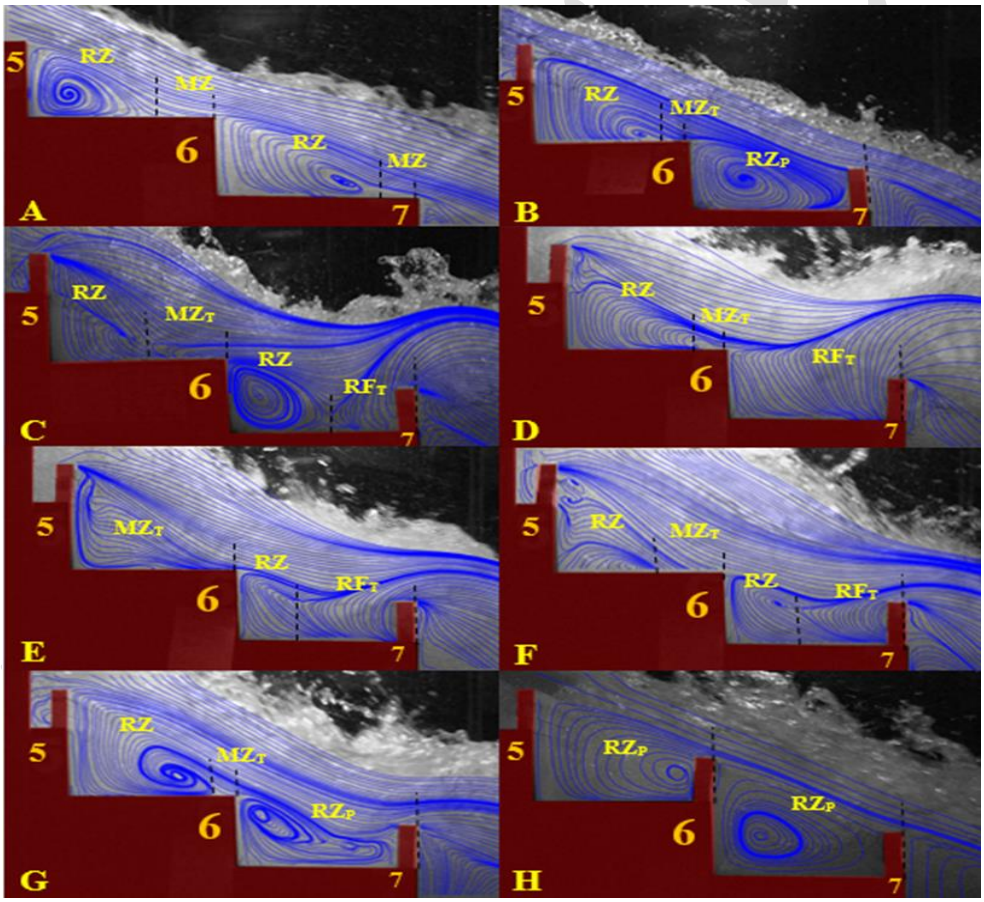


Fig. 13- Comparison of flow zones on Steps 6 and 7 at h_o/h = 0.56 and dc/h = 1.06, 1V:2H slope: A, flat step; B, l_o/w = 0.05; C, 0.10; D, 0.20; E, 0.25; F, 0.33; G, 0.50; H, 1.00.

For investigation of the height effects, l_o/w = 0.25 was used because the highest dissipation was obtained at this relative length in the energy-dissipation analysis; for investigation of the length effects, h_o/h = 0.56 was used because it was identified as the optimal height (Figs. 12 and 13). RF, RFT, and MZT regions for l_o/w = 0.25 and dc/h = 1.06 are shown in Figure (12).Compared with continuous obstacles (RF and MZ in Fig. 11), larger RFT and MZT areas were produced by discontinuous obstacles, a larger portion of the steps was covered, and RZ was reduced under similar h_o/h and dc/h conditions. RZP was not formed in the discontinuous configuration because flow passage between the obstacles was permitted. For h_o/h = 0.56 (Fig. 13), the combined RFT + MZT area across consecutive steps was expanded as l_o/w was increased from 0.1 to 0.33, and a maximum was reached at l_o/w = 0.25. At l_o/w = 0.5 or 0.05, RZP was formed in a manner similar to that observed for continuous obstacles.

Flow pattern

Variations in surface flow patterns were observed with discontinuous-obstacle length, height, flow regime, and slope, and differences from the flat-step and continuous configurations were identified. At l_o/w = 0.5, the patterns were characterized by sidewall standing waves, shockwaves, and wavy flow (Guenther et al., 2013). At l_o/w = 0.05–0.33, single-path waves were transformed into multi-path waves, and staggered patterns were created by upward flow in unobstructed areas (Fig. 14). At l_o/w = 0.05 in the upper transitional and skimming regimes, staggered effects were not observed because of the close obstacle spacing, and patterns resembling those of continuous obstacles were obtained.

Air cavities in transitional regimes varied depending on obstacle relative length and height and were categorized into three types:

- **Type I**: Constant-size air pocket across the full flume width, typical of flat step spillways (Guenther et al., 2013; Felder et al., 2012),
- **Type II**: Oscillating air pocket for continuous obstacles (Guenther et al., 2013),
- **Type III**: Oscillating air-water mixture pocket for discontinuous obstacles, characterized by dimensional oscillations and enhanced mixing fed by jets over the obstacles and transverse flows from the sides.

Mixing intensity and flow rate in Type III cavities were lower at l_o/w = 0.5 than at l_o/w = 0.05–0.33 because the cavities at l_o/w = 0.05–0.33 were influenced by transverse flows from both sides, whereas at l_o/w = 0.5 they were fed only by the central transverse flow. Cavity dimensions were expanded with increasing h_o/h. This Type III cavity was observed at both slopes with varying intensities.

A summary of the surface flow patterns is provided in Table (4). Multi-wavy and staggered surface patterns were created by discontinuous obstacles with l_o/w = 0.1–0.33, and increased three-dimensional effects and aeration across the spillway width and length were thereby produced relative to l_o/w = 0.5, continuous-obstacle, or flat-step configurations.

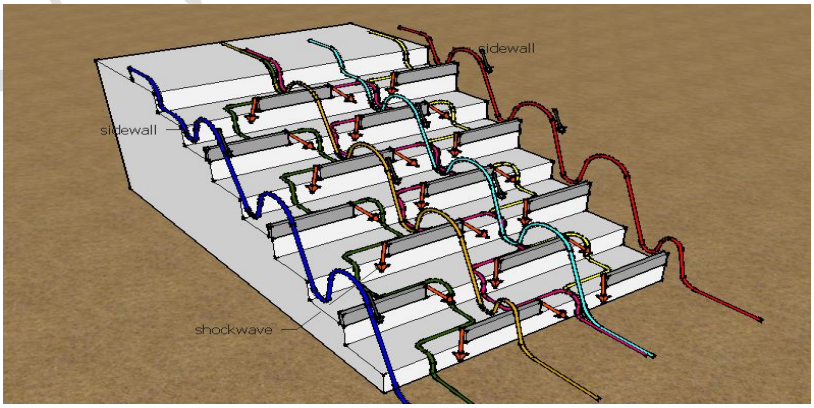


Fig. 14- Definition sketch of sidewall standing waves, shockwaves, wavy flow, and the staggered flow pattern for discontinuous obstacles at l_o/w = 0.25.

Table 4- Comparison of surface flow patterns for different configurations.

Regime	flat step	Continuous obstacle (l_o/w=1)	Discontinuous obstacle (l_o/w=0.5)	Discontinuous obstacle (l_o/w=0.05 to 0.33)
Nappe	Succession of free-falling flow	Succession of free-falling, pulsating flow in first step	Wavy flow pattern; higher obstacles strengthen waves and reduce passing flow; highly aerated jet; irregular sidewall standing waves and shockwaves; inclined surface over obstacle; three-dimensional flow.	Multi-wavy flow with transverse flow; distributed highly aerated jet; sidewall standing waves and shockwaves; highly three-dimensional flow; increased aeration with height (more than l_o/w = 0.5 at equal h_o/h); staggered flow pattern.
Transition	Air pocket; strong droplet splashing	Strong droplet splashing; oscillating air pocket	Some jets plunge over two steps; less wavy flow than nappe; oscillating air-water mixture pocket; highly aerated surface; three-dimensional flow; irregular sidewall standing waves and shockwaves.	Jets plunge over two steps (except l_o/w = 0.05); lower multi-wavy with transverse flow than nappe; highly oscillating air-water mixture pocket; more aerated surface than nappe and other configurations; highly three-dimensional flow; higher sidewall waves than l_o/w = 0.5 (l_o/w = 0.05 similar to continuous); shockwaves; staggered flow pattern.
Skimming	Transparent flow before IP; aerated after IP	Transparent before IP; aerated after IP; larger depth than flat step; horizontal surface at first step for highest obstacle.	Less transparent before IP than continuous; highly aerated with splashing after IP; lower sidewall effect than transitional; stronger shockwaves at higher obstacles; three-dimensional flow; unsteady/disturbed RZ.	Less transparent before IP than continuous (except l_o/w = 0.05 with RZ_P); highly aerated with splashing after IP; lower sidewall effect than transitional; highly three-dimensional flow; more unsteady/disturbed RZ than l_o/w = 0.5; staggered flow pattern (except l_o/w = 0.05).

Effects of Obstacle Dimensions on Relative Energy Dissipation

The overall energy dissipation for each configuration was evaluated using a global energy-balance approach. The difference between the upstream total head, calculated from the critical depth d_c at the spillway crest, and the residual head at the spillway toe was determined. The downstream energy was calculated using the initial conjugate depth y_1 associated with a classical hydraulic jump formed at the spillway toe, consistently with the procedure applied by Habibi et al. (2025). The energy drop ΔH and relative energy dissipation $\Delta H/H_t$ are defined by Equations (1) and (2), respectively.

$$\Delta H = H_t - H_1 = (1.5\, d_c + H) - [y_1 + V_1^2/(2g)] \quad (1)$$

The relative energy-dissipation efficiency is defined as:

$$\Delta H/H_t = (H_t - H_1)/H_t = 1 - H_1/H_t = 1 - [y_1 + V_1^2/(2g)]/(1.5\, d_c + H) \quad (2)$$

where V_1 is the mean supercritical velocity at the spillway toe, y_1 is the initial conjugate depth, d_c is the critical depth at the crest, H is the total spillway height, H_1 is the residual energy head, H_t is the upstream total head, g is gravitational acceleration, and ΔH is the energy drop. In every experiment, the downstream gate was adjusted so that a classical hydraulic jump began at the start of the stilling basin, with the jump toe located at

the spillway toe. The sequent tailwater depth y_2 was measured with the point gauge. Because the approach flow was turbulent and aerated, y_1 was not measured directly; instead, it was obtained from the measured y_2 and the known unit discharge q by solving the Bélanger conjugate-depth relation, $y_2/y_1 = 0.5[\sqrt{(1 + 8Fr_1^2)} - 1]$, where $Fr_1 = q/\sqrt{(g\, y_1^3)}$. The mean toe velocity was subsequently calculated from continuity as $V_1 = q/y_1$. The numerical results are provided in Appendix Tables (A2) and (A3).

This global methodology was selected for its robustness and widespread use in the literature, and a reliable basis for the relative comparison of different hydraulic-structure designs is thereby provided. It is acknowledged that air entrainment and turbulence are accounted for more comprehensively by advanced empirical models, such as those proposed by Chanson (2002) and Boes and Hager (2003b) and synthesized in the recent comprehensive review by Bekheet et al. (2025). However, detailed void-fraction data are required for their application, and such data were not collected in this study. Moreover, energy dissipation in highly aerated flows may be underestimated by the global approach because of the inherent complexities associated with defining and measuring energy in a two-phase air-water mixture, a limitation highlighted in recent literature (Sánchez-Juny et al., 2022; Valero et al., 2024). Given these considerations, the global energy-balance method was deemed the most appropriate and rigorous approach for achievement of the primary objective of this study: a comparative performance assessment of the different obstacle configurations.

The energy-dissipation results for the 1V:2H and 1V:3H spillways are summarized in Appendix Tables (A2) and (A3), respectively.

The effects of obstacle discontinuity were first examined on the 1V:3H spillway. As the discontinuous-obstacle height was increased, energy dissipation was enhanced up to a threshold; no systematic improvement was obtained beyond $h_o/h = 0.56$ within the tested range. Accordingly, $h_o/h = 0.56$ was identified as the optimum height (Fig. 15; Appendix Table A3). In the nappe-flow regime, changes in energy dissipation were generally smaller than 4 percentage points because a large fraction of the available energy was already dissipated by the stepped geometry. Larger improvements were obtained in the upper transitional and skimming-flow regimes, where intensified mixing was produced by the discontinuous obstacles.

For the upper transitional and skimming-flow regimes ($d_c/h \geq 0.83$), energy dissipation at the optimum height $h_o/h = 0.56$ increased as l_o/w was increased to 0.25 and decreased at greater lengths (Fig. 16). Therefore, the highest dissipation in these regimes on the 1V:3H spillway was obtained at $l_o/w = 0.25$ and $h_o/h = 0.56$. For nappe and lower transitional flow, $l_o/w = 0.10$ was generally more effective. Most discontinuous configurations outperformed the flat-step and continuous-obstacle configurations, particularly at higher d_c/h; however, small or negligible improvements were obtained for several low-discharge cases (Appendix Table A3).

For the 1V:2H spillway, a reduced subset of configurations was tested after the 1V:3H results had been screened. As on the milder slope, $h_o/h = 0.56$ was identified as the optimum height (Fig. 17). At this height, energy dissipation increased as l_o/w was increased to 0.25 and decreased at greater values (Fig. 18). At the higher d_c/h values, $l_o/w = 0.50$ did not produce a consistent improvement over the flat-step configuration, in agreement with the trend reported by Guenther et al. (2013).

When the energy-dissipation results were linked to the BIV observations and surface-flow patterns, a central transverse wavy path was identified at $l_o/w = 0.50$. As l_o/w was reduced to 0.10–0.33, additional wavy paths and staggered surface patterns were generated, and both aeration and three-dimensional mixing were intensified. The combined $RF_T + MZ_T$ area across consecutive steps was greatest near $l_o/w = 0.25$ and $h_o/h = 0.56$, which corresponded to the maximum measured dissipation on both slopes. At $d_c/h = 1.06$, the optimum configuration increased dissipation by 19.11 percentage points on the 1V:3H spillway and by 9.41 percentage points on the 1V:2H spillway. These gains correspond to relative improvements of 41.5%

and 23.7%, respectively, while the final dissipation level on the milder slope exceeded that on the steeper slope by 16.05 percentage points.

The observed energy-dissipation trends are explained by the culmination of these hydrodynamic changes. A direct correlation was found between the maximum dissipation at l_o/w = 0.25 and h_o/h = 0.56 (Figs. 16, 18), the maximal spatial extent of the RF_T + MZ_T zones observed in the BIV results, and the most intense staggered-flow patterns. It is confirmed by this synergy that the enhanced three-dimensionality and aeration induced by optimally configured discontinuous obstacles are the primary mechanisms through which superior energy dissipation is produced.

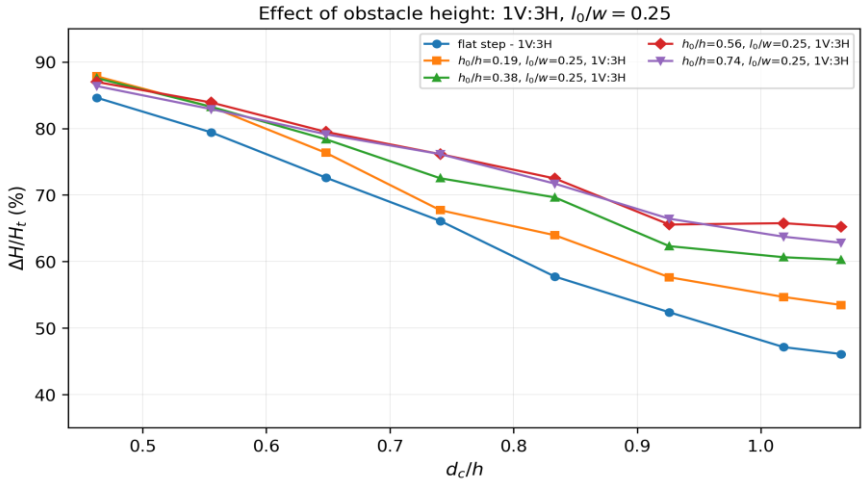


Fig. 15- Effect of obstacle height on relative energy dissipation for the 1V:3H spillway at l_o/w = 0.25.

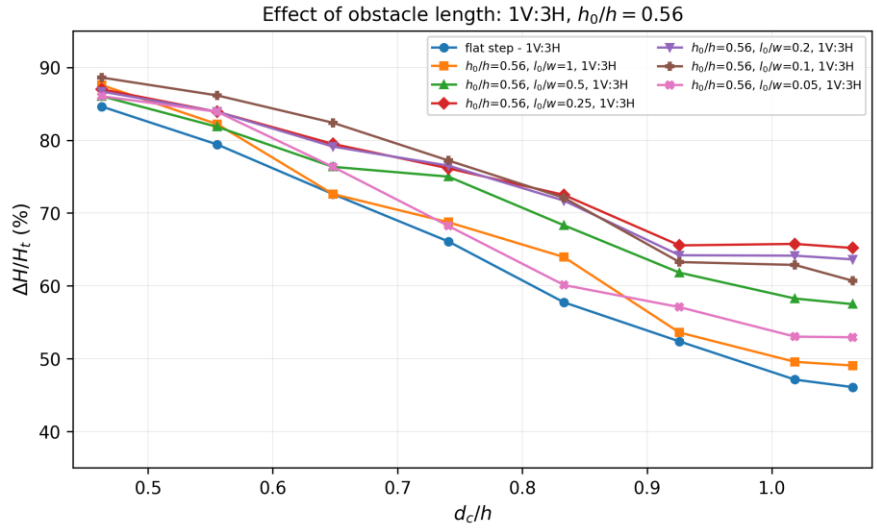


Fig. 16- Effect of obstacle length on relative energy dissipation for the 1V:3H spillway at h_o/h = 0.56.

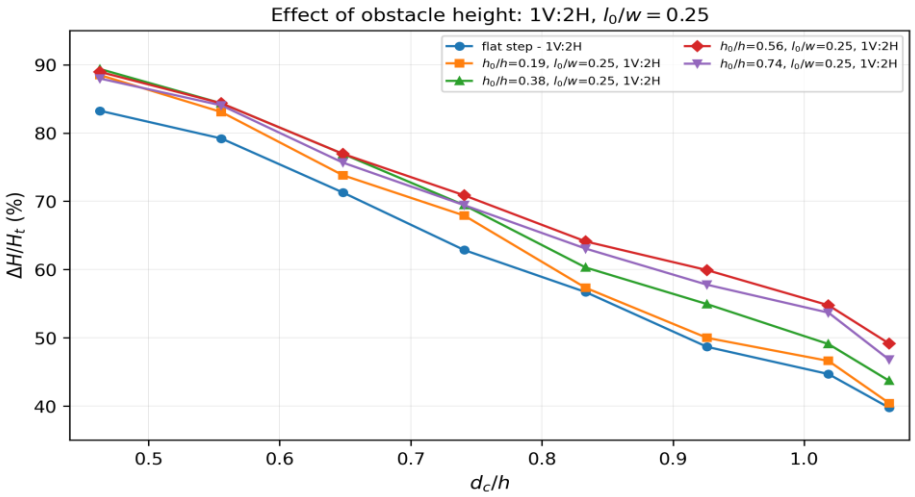


Fig. 17- Effect of obstacle height on relative energy dissipation for the 1V:2H spillway at $l_0/w = 0.25$.

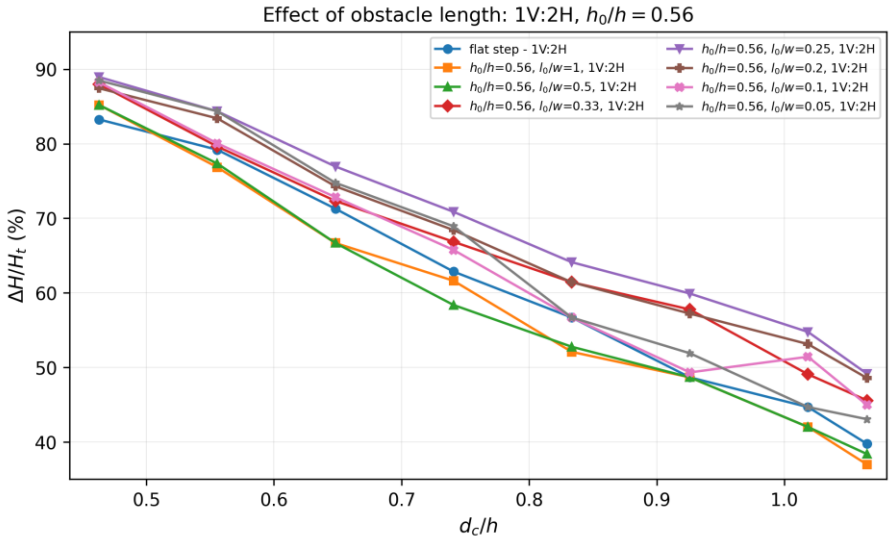


Fig. 18- Effect of obstacle length on relative energy dissipation for the 1V:2H spillway at $h_0/h = 0.56$.

Comparison with Previously Proposed Energy-Dissipation Methods

Previous modifications of stepped spillways can be classified according to their dominant energy-dissipation mechanisms. Through triangular protrusions, flow is redirected laterally and the effective chute roughness is increased. Earlier aeration inception and reduced downstream scour were reported by Wright (2010), although performance was found to be sensitive to obstacle spacing and the downstream-apron configuration. Cavity recirculation and jet interaction are enhanced by pooled, in-line, and staggered step arrangements. However, conventional flat steps were not necessarily outperformed by these configurations, and unstable cavity ejections, jump waves, transverse non-uniformities, and local flow concentrations were reported by Felder et al. (2012) and Guenther et al. (2013). Greater energy dissipation was produced by edge-mounted baffles than by end sills in the experiments of Zare and Doering (2012), while the effect of moving these elements away from the step edge was shown to depend on whether the edge was sharp or rounded. Increased energy dissipation in both nappe and skimming flows was obtained through inclined steps combined with end sills by Hamedi et al. (2014); nevertheless, the improvement was greater in nappe flow, and thinner end sills were more effective.

The available findings also indicate that hydraulic performance is not necessarily improved by increasing step complexity or porosity. Cavity recirculation was weakened and form drag was reduced when porous pool

walls were used by Felder and Chanson (2014). Consequently, the residual energy was approximately 1.3 times that of flat steps for a pool-wall porosity of 5% and approximately 1.5–2.0 times that of flat steps for a porosity of 31%, indicating lower energy dissipation. Energy dissipation was also found to decrease with increasing discharge and to be strongly affected by chute slope. In contrast, greater energy dissipation was obtained with the breakers investigated by Abdel Aal et al. (2018) because the flow was divided into interacting jets. The best performance was obtained at a relative breaker height of approximately 0.8, while the largest energy loss was generated by a perforated breaker with an opening area of approximately 5% and three openings. However, differences among the breaker configurations were reduced at larger discharges. Thus, a modification that is effective under nappe or transitional flow may become less effective after skimming flow has been established.

Gabion stepped spillways represent another important class of energy-dissipation structures because overflow and seepage are both permitted through their porous bodies. A reduction of approximately 10–30% in the required stilling-basin length was reported by Peyras et al. (1992) as a result of energy pre-dissipation along gabion steps. Energy-loss ratios for gabion-stepped weirs were reported by Chinnarasri et al. (2008) to be approximately 7%, 10%, and 14% greater than those of corresponding conventional stepped weirs for chute angles of 30°, 45°, and 60°, respectively. Gabion-step performance was found by Salmasi et al. (2012) to depend on porosity, chute slope, and the location of the impervious covering. Under the tested conditions, dissipation was generally enhanced by higher porosity and the milder 1V:2H slope, while impermeable vertical faces were more effective than impermeable horizontal coverings.

The hydraulic performance of gabion steps is strongly dependent on flow regime. Modification of cavity recirculation by seepage through porous steps was observed by Wüthrich and Chanson (2014). Under skimming-flow conditions, higher downstream velocities, lower flow resistance, and less energy dissipation were produced by the gabion chute than by the corresponding impermeable stepped chute. Similarly, the average friction factor of gabion steps in transitional and skimming flows was found by Zhang and Chanson (2016) to be approximately half that of smooth impermeable steps. Part of the surface-recirculation mechanism may therefore be bypassed by seepage as the gabion body approaches saturation. Conversely, conventional gabion steps were shown by Reeve et al. (2019) to perform better than overlapping, inclined, and pooled gabion geometries under otherwise identical numerical conditions. Greater energy dissipation was also obtained with short gabion spillways than with geometrically similar rigid spillways by Rajaei et al. (2020), although the relative efficiency of both configurations decreased as discharge increased.

The configuration- and regime-dependent advantages of gabion steps have been confirmed in more recent studies. For d_{50} = 10 mm, energy dissipation on a 1V:2H gabion stepped spillway was reported by Salmasi et al. (2023) to be approximately 30–35% greater than that obtained on a 1V:1H spillway. Rectangular end sills were also found to produce approximately 3–4% greater energy loss than inclined end sills. A maximum energy dissipation of 74.4% was obtained by Daneshfaraz et al. (2024) when gabions were installed on all steps, representing an increase of approximately 5.03% relative to solid steps. This advantage was mainly observed in nappe flow and diminished or was reversed after skimming flow developed. In a subsequent parametric investigation, the best gabion layout was reported by Daneshfaraz et al. (2026) to dissipate approximately 5% more energy than solid steps and to reduce the dimensionless residual head from approximately 4.65 to 4.21.

Larger improvements have been achieved by combining gabion steps with additional macro-roughness. An increase of up to 45.83% in relative energy dissipation, compared with unobstructed gabion steps, was reported by Sharma and Jhamnani (2025) when vertical obstructions were installed on the gabion steps. Greater energy dissipation

was subsequently obtained with triangular-sill gabion steps than with both conventional gabion and rigid stepped configurations (Sharma and Jhamnani, 2026), although optimum performance remained dependent on chute slope, sill dimensions, and discharge. These studies are particularly relevant to the present investigation because substantially greater energy loss than that produced by permeability alone was shown to result from the interaction between step permeability and discrete macro-roughness.

A strict ranking based on absolute energy-dissipation percentages would be misleading because different chute slopes, step dimensions and numbers, discharge ranges, flow regimes, downstream controls, porosities, and energy-reference sections were used among the studies. A more transparent comparison can be made by expressing the improvement relative to the reference configuration adopted in each investigation. Under the present conditions, the optimum discontinuous-obstacle arrangement (l_o/w = 0.25 and h_o/h = 0.56) increased energy dissipation at d_c/h = 1.06 from 46.09% to 65.20% on the 1V:3H chute. The resulting gain was 19.11 percentage points, corresponding to a 41.5% improvement relative to the flat-step value. On the 1V:2H chute, dissipation was increased from 39.74% to 49.15%, corresponding to a gain of 9.41 percentage points or a relative improvement of 23.7%.

The relative improvement obtained on the milder slope was greater than the approximately 5–14% improvements reported for several unmodified gabion-step arrangements and was of the same order as the maximum 45.83% improvement reported for gabion steps equipped with vertical obstructions. These values should not be interpreted as a universal ranking; rather, they provide a normalized benchmark because the experimental conditions differed. More importantly, the greatest improvements produced by the present discontinuous obstacles were obtained in the upper transitional and skimming-flow regimes, whereas the benefits of unmodified gabion steps and several end-sill configurations were generally greatest at lower discharges and decreased after skimming flow developed. The enhanced performance was attributed to simultaneous transverse exchange flows, multi-wavy and staggered surface patterns, Type III oscillating air–water cavities, and intensified three-dimensional mixing through the gaps between successive obstacles. Appropriately proportioned discontinuous obstacles can therefore provide an effective means of maintaining and increasing energy dissipation at relatively high discharges, particularly on mild-slope stepped spillways.

Conclusions

The effects of discontinuous edge obstacles on two stepped-spillway slopes were investigated experimentally, and the associated flow structures were analyzed using BIV. The principal conclusions are summarized as follows:

- The flat-step aeration-inception location was generally retained by discontinuous obstacles on the 1V:3H spillway, whereas selected larger obstacles shifted the inception point one step upstream on the 1V:2H spillway. Continuous obstacles shifted the inception point downstream.
- Skimming flow was promoted at lower d_c/h by continuous obstacles, whereas the transitional-flow range was extended and the discharge required for complete skimming was increased by discontinuous obstacles.
- RFT and MZT regions, transverse flow, multi-wavy surface patterns, and staggered three-dimensional flow were generated by discontinuous obstacles. The largest combined RF_T + MZ_T extent was obtained near l_o/w = 0.25 and h_o/h = 0.56.
- The optimum configuration within the tested range was l_o/w = 0.25 and h_o/h = 0.56. At d_c/h = 1.06, energy dissipation was increased from 46.09% to 65.20% on the 1V:3H spillway and from 39.74% to 49.15% on the 1V:2H spillway.
- Gains of 19.11 and 9.41 percentage points were obtained on the 1V:3H and 1V:2H spillways, respectively, corresponding to relative improvements of 41.5% and 23.7%. The greater effectiveness of the discontinuous obstacles on the milder slope was thereby demonstrated.
- The measured gains were associated with the enlarged RF_T + MZ_T zones, stronger

transverse exchange, and the most pronounced staggered-flow patterns. The proposed arrangement is therefore most applicable where energy dissipation must be maintained at upper transitional and skimming-flow discharges.

Limitations and Future Research

The present experiments were limited to $d_c/h \leq 1.06$, two chute slopes, and BIV measurements obtained near the sidewall between Steps 6 and 7. In addition, void-fraction and pressure-fluctuation measurements were not available; therefore, the global energy-balance method was used and flow-depth increases and sidewall-wave amplitudes could not be quantified systematically.

Future studies should be extended to higher d_c/h values and fully developed skimming flow, and scale effects should be assessed through geometrically scaled and prototype-scale testing. Full-width three-dimensional measurements should be performed using stereoscopic BIV/PIV, air-concentration probes, and synchronized pressure sensors so that transverse velocities, turbulence, void fraction, pressure fluctuations, cavitation potential, flow depth, and sidewall-wave amplitudes can be quantified. Additional obstacle shapes, transverse and longitudinal spacings, staggered layouts, edge curvatures, and permeable or gabion-based hybrid configurations should be examined. Experimentally validated three-dimensional numerical models should also be developed for multi-objective optimization of energy dissipation, freeboard, structural loading, and construction requirements. Finally, prototype applicability should be evaluated under sediment transport, floating debris, partial blockage, downstream scour, and long-term durability conditions.

Conflict of Interest

The authors declared no potential conflicts of interest concerning the research, authorship, and publication of this article. Confirmation.

Funding

The authors received no financial support for the research, authorship, and publication of this article.

Data Availability Statements

The datasets generated and/or analyzed during the current study are available from the corresponding author on reasonable request.

Declaration of Generative AI and AI-assisted technologies in the writing process

During preparation of this manuscript, the authors used OpenAI ChatGPT solely for English-language editing, consistency checking, and formatting. No generative AI was used to generate or analyze experimental data, results, or conclusions. The authors reviewed and approved all content and take full responsibility for the manuscript.

Authors' contribution

First Author: Seyed Amin Asghari Pari, conception and design; material preparation; data collection, analysis and interpretation; critical review and revision.

Second Author: Mojtaba Kordnaeij, conception and design; material preparation; data collection, analysis and interpretation; original draft preparation; revision.

Third Author: Ram Balachandar, conception and design; interpretation of results; supervision; critical review and revision.

Acknowledgment

This research has no acknowledgments.

List of Abbreviations and Symbols

Term	Definition
3D	three-dimensional
ADV	Acoustic Doppler Velocimetry
BIV	Bubble Image Velocimetry
IP	inception point of free-surface aeration
IPP	Image Processing Procedure
MZ	mixing zone
MZ_T	mixing zone modified by transverse flow
OF	Optical Flow
PIV	Particle Image Velocimetry
RF	redirected-flow zone
RF_T	redirected-flow zone modified by transverse flow
RZ	recirculation zone
RZ_P	pooled-step recirculation zone
VC	video correlation
d_c	critical flow depth at the spillway entrance
dc/h	relative critical depth
h	step height
h_o	obstacle height
h_o/h	relative obstacle height
H	total spillway height
H_1	residual energy head at the spillway toe
Ht	upstream total energy head
L	horizontal step length
l_o	obstacle length
l_o/w	relative obstacle length
N	number of steps
q	discharge per unit width
V_1	mean supercritical velocity at the spillway toe
w	flume width
y_1	initial (supercritical) conjugate depth of the hydraulic jump
y_2	sequent (tailwater) depth of the hydraulic jump
ΔH	energy drop across the spillway
θ	spillway inclination angle

References

1- Abdel Aal, G. M., Sobeah, M., Helal, E., and El-Fooly, M., 2018. Improving energy dissipation on stepped spillways using breakers. *Ain Shams Engineering Journal*, 9(4), 1887–1896. https://doi.org/10.1016/j.asej.2017.01.008

2- Amador, A., Sánchez-Tembleque, F., Sánchez-Juny, M., Puertas, J., and Dolz, J., 2004a. Velocity and pressure field in skimming flow in stepped spillways. *In Proceedings of the 9th International Conference on Hydraulic Engineering* (pp. 279–286).

3- Amador, A., Van der Graaf, G., Sánchez-Juny, M., Dolz, J., Sánchez-Tembleque, F., Puertas, J., and Girona, C. J., 2004b. Characterization of the flow field in a stepped spillway by PIV. In *Proceedings of the 12th Symposium on Applications of Laser Techniques to Fluid Mechanics* (pp. 12–15).

4- Andre, S., Boillat, J. L., Schleiss, A. J., and Matos, J., 2004. Energy dissipation and hydrodynamic forces of aerated flow over macro-roughness linings for overtopped embankment dams. *In Proceedings of the International Conference on Hydraulics of Dams and River Structures* (pp. 189–196).

5- Asghari Pari, S. A., and Kordnaeij, M., 2021. Laboratory examination of the effect of discontinuous obstacle on the edge of a stepped spillway. *Journal of Irrigation and Drainage Structures Engineering Research*, 22(83), 121–140. https://doi.org/10.22092/idser.2021.354709.1473 [In Persian].

6- Bekheet, A. A., AboulAtta, N. M., Saad, N. Y., and El-Molla, D. A., 2025. Energy dissipation in stepped spillways: A comprehensive review of the recent research. *Innovative Infrastructure Solutions, 10, Article 253*. https://doi.org/10.1007/s41062-025-02042-6

7- Boes, R. M., and Hager, W. H., 2003a. Two-phase flow characteristics of stepped spillways. *Journal of Hydraulic Engineering*, 129(9), 661–670. https://doi.org/10.1061/(ASCE)0733-9429(2003)129:9(661)

8- Boes, R. M., and Hager, W. H., 2003b. Hydraulic design of stepped spillways. *Journal of Hydraulic Engineering*, 129(9), 671–679. https://doi.org/10.1061/(ASCE)0733-9429(2003)129:9(671)

9- Bühler, P., Leandro, J., Bung, D., Lopes, P., and Carvalho, R., 2015. Measuring void fraction of a stepped spillway with non-intrusive methods using different image resolutions. *IWHS 2015*, 41.

10- Bung, D. B., and Valero, D., 2015. Image processing for bubble image velocimetry in self-aerated flows. *In Proceedings of the 36th IAHR World Congress* (pp. 6594–6601).

11- Bung, D. B., and Valero, D., 2016a. Image processing techniques for velocity estimation in highly aerated flows: Bubble Image Velocimetry vs. Optical Flow. *In Proc. 4th IAHR Europe Congress* (pp. 151–157).

12- Bung, D. B., and Valero, D., 2016b. Optical flow estimation in aerated flows. *Journal of Hydraulic Research*, 54(5), 575–580. https://doi.org/10.1080/00221686.2016.1173600

13- Chang, K. A., and Liu, P. L. F., 1998. Velocity, acceleration and vorticity under a breaking wave. *Physics of Fluids*, 10(1), 327–329. https://doi.org/10.1063/1.869544

14- Chanson, H., 1995. Hydraulic design of stepped cascades, channels, weirs and spillways. Pergamon.

15- Chanson, H., 2001. Hydraulic design of stepped spillways and downstream energy dissipators. *Dam Engineering*, 11, 205–242.

16- Chanson, H., 2002. The hydraulics of stepped chutes and spillways. CRC Press.

17- Chanson, H., 2006. Hydraulics of skimming flows on stepped chutes: The effects of inflow conditions? *Journal of Hydraulic Research*, 44(1), 51–60. https://doi.org/10.1080/00221686.2006.9521655

18- Chanson, H., 2022. Stepped spillway prototype operation and air entrainment: Toward a better understanding of the mechanisms leading to air entrainment in skimming flows. *Journal of Hydraulic Engineering*, 148(12), 05022004. https://doi.org/10.1061/(ASCE)HY.1943-7900.0002018

19- Chanson, H., Bung, D. B., and Matos, J., 2015. Stepped spillways and cascades. *IAHR Monograph. School of Civil Engineering, University of Queensland*.

20- Chinnarasri, C., Donjadee, S., and Israngkura, U., 2008. Hydraulic characteristics of gabion-stepped weirs. *Journal of Hydraulic Engineering*, 134(8), 1147–1152. https://doi.org/10.1061/(ASCE)0733-9429(2008)134:8(1147)

21- Daneshfaraz, R., Ghaderi, A., Sadeghi, H., Mohammadnezhad, H., and Abraham, J. P., 2026. Hydraulic behavior and dissipation of energy in stepped spillways with gabion steps. *Water Resources Management*, 40, Article 352. https://doi.org/10.1007/s11269-026-04755-4

22- Daneshfaraz, R., Sadeghi, H., Ghaderi, A., and Abraham, J. P., 2024. The effect of gabion steps on the hydraulic jump characteristics downstream of stepped spillways. *Water Science*, 38, 128–139. https://doi.org/10.1080/23570008.2024.2307243

23- Emadzadeh, A., and Chiew, Y. M., 2017. Bubble dynamics and PIV measurements in a hydraulic jump. In *Proceedings of the 37th IAHR World Congress* (pp. 1–10).

24- Felder, S., 2013. Air-water flow properties on stepped spillways for embankment dams: Aeration, energy dissipation and turbulence on uniform, non-uniform and pooled stepped chutes [Doctoral dissertation, University of Queensland].

25- Felder, S., and Chanson, H., 2014. Effects of step pool porosity upon flow aeration and energy dissipation on pooled stepped spillways. *Journal of Hydraulic Engineering*, 140(4), 04014002. https://doi.org/10.1061/(ASCE)HY.1943-7900.0000858

26- Felder, S., and Chanson, H., 2015. Air–water flow properties in the developing flow region of a stepped spillway with porous pooled steps. *Journal of Hydraulic Engineering*, 141(9), 04015020. https://doi.org/10.1061/(ASCE)HY.1943-7900.0001037

27- Felder, S., and Chanson, H., 2016. Simple design criterion for residual energy on embankment dam stepped spillways. *Journal of Hydraulic Engineering*, 142(2), 04015062. https://doi.org/10.1061/(ASCE)HY.1943-7900.0001098

28- Felder, S., Fromm, C., and Chanson, H., 2012. Air entrainment and energy dissipation on a 8.9° slope stepped spillway with flat and pooled steps. *Journal of Hydraulic Engineering*, 138(10), 878–885. https://doi.org/10.1061/(ASCE)HY.1943-7900.0000599

29- Frizell, K. W., Renna, F. M., and Matos, J., 2013. Cavitation potential of flow on stepped spillways. *Journal of Hydraulic Engineering*, 139(6), 630–636. https://doi.org/10.1061/(ASCE)HY.1943-7900.0000715

30- Gonzalez, C. A., and Chanson, H., 2007. Hydraulic design of stepped spillways and downstream energy dissipators for embankment dams. *Dam Engineering*, 17(4), 223–244.

31- Gonzalez, C. A., Takahashi, M., and Chanson, H., 2005. Effects of step roughness in skimming flows: An experimental study. *Journal of Hydraulic Research*, 43(3), 287–297. https://doi.org/10.1080/00221686.2005.9641235

32- Guenther, P., Felder, S., and Chanson, H., 2013. Flow aeration, cavity processes and energy dissipation on flat and pooled stepped spillways for embankments. *Environmental Fluid Mechanics*, 13(5), 503–525. https://doi.org/10.1007/s10652-013-9277-4

33- Habibi, K., Erfani Fard, F., Asghari Pari, S. A., and Azimi, A. H., 2025. Experimental and numerical studies on the hydraulics of stepped spillways with baffle walls and blocks. *ISH Journal of Hydraulic Engineering*, 31(2), 217–238. https://doi.org/10.1080/09715010.2025.2471339

34- Hamedi, A., Mansoori, A., Shamsai, A., and Amirahmadian, S., 2014. Effects of end sill and step slope on stepped spillway energy dissipation. *Journal of Water Sciences Research*, 6(1), 1–15.

35- Hunt, S. L., and Kadavy, K. C., 2010. Energy dissipation on flat-sloped stepped spillways: Part 1. Upstream of the inception point. *Transactions of the ASABE*, 53(1), 103–109. https://doi.org/10.13031/2013.29497

36- Kordnaeij, M., Asghari Pari, S. A., and Falahat, H., 2023. Energy dissipation on stepped spillways: The effect of mounted step roughness. *In Proceedings of the 40th IAHR World Congress*, Vol. 21, p. 25.

37- Kramer, M., and Chanson, H., 2018a. Transition flow regime on stepped spillways: Air–water flow characteristics and step-cavity fluctuations. *Environmental Fluid Mechanics*, 18, 947–965. https://doi.org/10.1007/s10652-018-9575-y

38- Kramer, M., and Chanson, H., 2018b. Free-surface instabilities in high-velocity air-water flows down stepped chutes. *Journal of Hydraulic Research*, 56(6), 825–841. https://doi.org/10.1080/00221686.2018.1436859

39- Krisnayanti, D. S., Soehardjono, Dermawan, V., and Sholichin, M., 2016. Flow and energy dissipation over on flat and pooled stepped spillway. *Journal Teknologi (Sciences & Engineering)*, 78(8), 79–86. https://doi.org/10.11113/jt.v78.5973

40- Kökpinar, M. A., 2004. Flow over a stepped chute with and without macro-roughness elements. Canadian *Journal of Civil Engineering*, 31(5), 880–891. https://doi.org/10.1139/l04-037

41- Leandro, J., Bung, D. B., and Carvalho, R., 2014. Measuring void fraction and velocity fields of a stepped spillway for skimming flow using non-intrusive methods. *Experiments in Fluids*, 55(5), 1732. https://doi.org/10.1007/s00348-014-1732-6

42- Li, S., and Zhang, J., 2018. Numerical investigation on the hydraulic properties of the skimming flow over pooled stepped spillway. *Water*, 10(10), 1478. https://doi.org/10.3390/w10101478

43- Li, S., Zhang, J., and Xu, W., 2018. Numerical investigation of air–water flow properties over steep flat and pooled stepped spillways. *Journal of Hydraulic Research*, 56(1), 1–14. https://doi.org/10.1080/00221686.2017.1286393

44- Lopes, P., Bung, D. B., and Leandro, J., 2017. Alternating skimming flow over a stepped spillway. *Environmental Fluid Mechanics*, 17(2), 303–322. https://doi.org/10.1007/s10652-016-9477-9

45- Lopes, P., Bung, D. B., Leandro, J., and Carvalho, R. F., 2015. The effect of cross-waves in physical stepped spillway models. *In E-proceedings of the 36th IAHR World Congress*.

46- Meireles, I., and Matos, J., 2009. Skimming flow in the nonaerated region of stepped spillways over embankment dams. *Journal of Hydraulic Engineering*, 135(8), 685–689. https://doi.org/10.1061/(ASCE)HY.1943-7900.0000058

47- Mikalsen, L. and Thorsen, K., 2023. *Improved Energy Dissipation in Stepped Spillways—Hydraulic Model Study Applying Bubble Image Velocimetry* (Doctoral dissertation, NTNU).

48- Mikalsen, L. M., Thorsen, K. H., Bor, A., and Lia, L., 2024. Investigation of Improved Energy Dissipation in Stepped Spillways Applying Bubble Image Velocimetry. *Water*, 16(17), 2432. https://doi.org/10.3390/w16172432

49- Ohtsu, I., and Yasuda, Y., 1997. Characteristics of flow conditions on stepped channels. *In Proceedings of the 27th Congress of IAHR* (pp. 583–588).

50- Ostad Mirza, M.J., 2016. *Experimental study on the influence of abrupt slope changes on flow characteristics over stepped spillways* (Doctoral dissertation, EPFL).

51- Peyras, L., Royet, P., and Degoutte, G., 1992. Flow and energy dissipation over stepped gabion weirs. *Journal of Hydraulic Engineering*, 118(5), 707–717. https://doi.org/10.1061/(ASCE)0733-9429(1992)118:5(707)

52- Rajaei, S. H., Khodashenas, S. R., and Esmaili, K., 2020. Comparative evaluation of energy dissipation over short stepped gabion and rigid spillways. *Journal of Hydraulic Research*, 58(2), 262–273. https://doi.org/10.1080/00221686.2019.1572661

53- Reeve, D. E., Zuhaira, A. A., and Karunarathna, H., 2019. Computational investigation of hydraulic performance variation with geometry in gabion stepped spillways. *Water Science and Engineering*, 12(1), 62–72. https://doi.org/10.1016/j.wse.2019.04.002.

54- Ryu, Y., Chang, K. A., and Lim, H. J., 2005. Use of bubble image velocimetry for measurement of plunging wave impinging on structure and associated greenwater. *Measurement Science and Technology*, 16(10), 1945–1953. https://doi.org/10.1088/0957-0233/16/10/011

55- Salmasi, F., Razi, S., and Abraham, J. P., 2023. Hydraulics of flow in gabion stepped spillways: An experimental study. *Journal of Hydraulic Structures*, 9(2), 75–100. https://doi.org/10.22055/jhs.2023.40421.1257

56- Salmasi, F., Sattari, M. T., and Pal, M., 2012. Application of data mining on evaluation of energy dissipation over low gabion-stepped weir. Turkish *Journal of Agriculture and Forestry*, 36(1), 95–106. https://doi.org/10.3906/tar-1011-1506

57- Sharma, A. K., and Jhamnani, B., 2025. Enhancing energy dissipation with vertical obstructions on gabion stepped spillways. *National Academy Science Letters. Advance online publication*. https://doi.org/10.1007/s40009-025-01873-2

58- Sharma, A. K., and Jhamnani, B., 2026. Experimental and soft computing analysis of hydraulic performance in gabion stepped spillways: A comparative study. *Proceedings of the National Academy of Sciences, India Section A: Physical Sciences*. Advance online publication. https://doi.org/10.1007/s40010-026-01054-w

59- Sánchez-Juny, M., Estrella, S., Matos, J., Bladé, E., Martínez-Gomariz, E., and Bonet Gil, E., 2022. Velocity measurements in highly aerated flow on a stepped chute without sidewall constraint using a BIV technique. *Water*, 14(16), 2587. https://doi.org/10.3390/w14162587

60- Valero, D., Felder, S., Kramer, M., Wang, H., Carrillo, J. M., Pfister, M., and Bung, D. B., 2024. Air–water flows. *Journal of Hydraulic Research*, 62(4), 319–339. https://doi.org/10.1080/00221686.2024.2343261

61- Wright, H. J., 2010. Improved energy dissipation on stepped spillways with the addition of triangular protrusions. *In Proceedings of the 78th ICOLD Annual Meeting* (pp. 1–10).

62- Wüthrich, D., and Chanson, H., 2014. Hydraulics, air entrainment, and energy dissipation on a gabion stepped weir. *Journal of Hydraulic Engineering*, 140(9), 04014046. https://doi.org/10.1061/(ASCE)HY.1943-7900.0000919

63- Zare, H. K., and Doering, J. C., 2012. Energy dissipation and flow characteristics of baffles and sills on stepped spillways. *Journal of Hydraulic Research*, 50(2), 192–199. https://doi.org/10.1080/00221686.2012.661916

64- Zhang, G., and Chanson, H., 2016. Gabion stepped spillway: Interactions between free-surface, cavity, and seepage flows. *Journal of Hydraulic Engineering*, 142(5), 06016002. https://doi.org/10.1061/(ASCE)HY.1943-7900.0001120

65- Zhang, G., and Chanson, H., 2018. Application of local optical flow methods to high-velocity free-surface flows: Validation and application to stepped chutes. *Experimental Thermal and Fluid Science*, 90, 186–199. https://doi.org/10.1016/j.expthermflusci.2017.09.010.

Appendix A. Supplementary Data Tables

Table A1. Step number of the free-surface aeration inception point for different obstacle arrangements at d_c/h = 1.06.

dc/h= 1.06	flat step	l_o/w = 1				l_o/w = 0.05				l_o/w = 0.1				l_o/w = 0.2				l_o/w = 0.25				l_o/w = 0.33				l_o/w = 0.5			
		h_o/h				h_o/h				h_o/h				h_o/h				h_o/h				h_o/h				h_o/h			
		0.19	0.38	0.56	0.74	0.19	0.38	0.56	0.74	0.19	0.38	0.56	0.74	0.19	0.38	0.56	0.74	0.19	0.38	0.56	0.74	0.19	0.38	0.56	0.74	0.19	0.38	0.56	0.74
θ=19.2	4	5	5	5	5	4	4	5	---	4	4	4	4	4	4	4	4	4	4	4	4	---	---	---	---	4	4	4	3
θ=27.5	5	6	6	6	---	5	6	6	6	5	5	5	---	5	4	4	---	5	5	4	4	5	4	4	---	5	4	4	---

Note: A dash indicates that the corresponding configuration was not tested.

Table A2. Relative energy dissipation (%) for different step configurations on the 1V:2H spillway (θ = 27.5°).

dc/h	θ	flat step	l_o/w = 1			l_o/w = 0.05				l_o/w = 0.1			l_o/w = 0.2			l_o/w = 0.25				l_o/w = 0.33			l_o/w = 0.5		
			h_o/h			h_o/h				h_o/h			h_o/h			h_o/h				h_o/h			h_o/h		
			0.19	0.38	0.56	0.19	0.38	0.56	0.74	0.19	0.38	0.56	0.19	0.38	0.56	0.19	0.38	0.56	0.74	0.19	0.38	0.56	0.19	0.38	0.56
0.46	27.5	83.26	87.44	85.90	85.20	87.15	88.24	88.49	88.95	87.44	87.72	88.24	87.98	87.98	87.44	88.49	89.38	88.95	87.98	87.44	87.72	87.98	86.86	85.90	85.20
0.55	27.5	79.20	78.75	77.83	76.86	77.83	82.73	84.36	85.75	78.30	79.63	80.06	81.26	82.73	83.41	83.08	84.36	84.36	84.05	80.47	80.06	79.63	78.30	77.35	77.35
0.64	27.5	71.29	66.69	68.50	66.69	66.69	74.76	74.76	75.67	67.30	71.29	72.84	73.82	75.67	74.30	73.82	76.95	76.95	75.67	69.64	72.33	72.33	66.69	67.30	66.69
0.73	27.5	62.85	61.62	62.85	61.62	59.04	67.38	68.93	71.33	54.12	58.37	65.75	66.31	68.42	68.42	67.91	69.43	70.87	69.43	65.19	65.75	66.85	60.99	59.70	58.37
0.83	27.5	56.69	57.32	54.12	52.09	51.39	54.12	56.69	64.63	43.09	49.24	56.69	57.32	59.72	61.43	57.32	60.29	64.11	63.06	55.42	59.13	61.43	56.06	52.09	52.77
0.92	27.5	48.67	49.33	48.67	48.67	48.00	48.67	51.90	50.63	45.23	49.33	49.33	51.90	54.93	57.22	49.98	54.93	59.91	57.77	50.63	53.74	57.77	49.33	48.00	48.67
1.01	27.5	44.68	42.01	41.32	42.01	42.01	43.36	44.68	44.02	45.97	48.47	51.43	48.47	49.67	53.13	46.61	49.08	54.76	53.68	42.69	47.23	49.08	42.01	41.32	42.01
1.06	27.5	39.74	38.37	36.97	36.97	41.09	42.40	43.05	42.40	41.75	43.69	44.95	43.05	46.79	48.57	40.42	43.69	49.15	46.79	37.67	42.40	45.57	36.97	37.67	38.37

Note: A dash indicates that the corresponding configuration was not tested.

Table A3- Relative energy dissipation (%) for different step configurations on the 1V:3H spillway (θ = 19.2°).

dc/h	θ	Flat step	l_o/w = 1				l_o/w = 0.05			l_o/w = 0.1				l_o/w = 0.2				l_o/w = 0.25				l_o/w = 0.5			
			h_o/h				h_o/h			h_o/h				h_o/h				h_o/h				h_o/h			
			0.19	0.38	0.56	0.74	0.19	0.38	0.56	0.19	0.38	0.56	0.74	0.19	0.38	0.56	0.74	0.19	0.38	0.56	0.74	0.19	0.38	0.56	0.74
0.46	19.2	84.63	86.37	87.29	87.57	87.29	84.63	86.69	86.05	88.36	88.11	88.61	87.29	87.57	87.29	86.69	86.37	87.85	87.57	86.99	86.37	86.37	87.29	86.05	84.24
0.55	19.2	79.41	79.41	81.46	82.20	81.46	81.46	83.90	83.90	83.90	85.10	86.15	85.37	83.25	83.90	83.90	82.56	83.25	83.25	83.90	82.91	81.07	82.91	81.84	80.67
0.64	19.2	72.61	70.51	72.61	72.61	72.61	75.47	77.19	76.35	77.19	79.13	82.41	81.81	75.47	78.38	79.13	79.13	76.35	78.38	79.49	79.13	74.08	75.91	76.35	75.02
0.73	19.2	66.10	68.74	67.71	68.74	62.01	66.10	68.74	68.23	68.74	70.22	77.22	75.39	68.23	71.62	76.51	75.39	67.71	72.51	76.14	76.14	67.71	76.14	75.00	72.95
0.83	19.2	57.74	57.74	62.35	63.95	53.24	58.94	61.81	60.11	60.69	64.97	72.10	70.07	62.35	68.32	71.70	71.70	63.95	69.64	72.48	71.70	64.97	69.21	68.32	64.97
0.92	19.2	52.37	52.37	52.37	53.59	49.82	56.52	57.63	57.08	55.95	59.78	63.27	62.31	56.52	65.56	64.20	65.11	57.63	62.31	65.56	66.43	57.08	64.20	61.81	60.81
1.01	19.2	47.12	47.74	48.35	49.56	45.85	50.16	51.32	53.02	51.32	57.76	62.87	62.00	53.02	62.00	64.14	62.87	54.66	60.64	65.76	63.73	54.12	59.23	58.26	56.75
1.06	19.2	46.09	46.69	47.29	49.05	45.47	50.20	51.86	52.94	51.31	57.00	60.69	60.69	53.47	60.25	63.63	62.82	53.47	60.25	65.20	62.82	53.47	58.89	57.48	56.51

Note: A dash indicates that the corresponding configuration was not tested.